

Moving Target Indication with Dual Frequency Millimeter Wave SAR

Maurice Rüegg*, Manfred Hägelen†, Erich Meier* and Daniel Nüesch*

*Remote Sensing Laboratories, University of Zürich, Switzerland, Email: mrueegg@geo.unizh.ch

†Forschungsgesellschaft für Angewandte Naturwissenschaften e.V. (FGAN-FHR), Wachtberg, Germany

Abstract—Ground moving target indication (GMTI) for synthetic aperture radar (SAR) provides information on non-static objects in a static ground scene. An efficient approach for GMTI is the use of multi-channel SAR systems for a space- and time-variant analysis of moving targets. This allows the indication, correction of position errors, and estimation of radial velocity components for moving targets in the SAR image. All three steps are possible because of the Doppler frequency shift in the radar signal caused by the radial target movement. Our work focuses on the millimeter wave (mmW) SAR system MEMPHIS with multi-channel amplitude-comparison monopulse data recording and the ability to use carrier frequencies of 35 and 94 GHz simultaneously, making it a dual frequency multi-channel SAR. Our discussions include mmW specific SAR GMTI considerations and an adaptive algorithm to collect information on moving targets with a mmW monopulse radar, and GMTI blind speed elimination and target velocity ambiguity resolving by dual frequency SAR. For an experiment with MEMPHIS, frequency spectra, processed SAR images with position corrected moving targets, and accurate target velocities and positions are presented to verify the developed algorithm.

I. INTRODUCTION

The effects of smearing and displacement of moving targets in synthetic aperture radar (SAR) imagery have long been known and are discussed in detail in [1]. Ground moving target indication (GMTI) with SAR has been a widely explored field of interest ever since. Techniques for detection, position correction, refocusing, and velocity measurements of moving targets include the use of single- as well as multi-channel SAR data. [2]–[4] give a good overview of some of them including multilooking, displaced phase center antenna (DPCA) processing, along-track interferometry (ATI), monopulse processing, and signal filtering by space time adaptive processing (STAP).

Monopulse processing for GMTI is often used tantamount to ATI in the SAR community [5]. We would like to make a distinction in that ATI refers to interferometric SAR (InSAR) and the direct comparison of two or more received data records [6] from multiple antennas while monopulse or $\Sigma\Delta$ processing is a general term often used for tracking radar systems and always specified through a sum data signal and one or more isochronous difference data signals [7]. Monopulse processing looks at the complex ratios between these multiple signals and is thus well suited for GMTI.

Using a millimeter wave (mmW) SAR sensor for GMTI experiments has several advantages as well as drawbacks. Among the advantages are the relatively small size of the sensor antenna and hardware—suitable for application in small

aircraft or drones—and a high GMTI sensitivity because of a short wavelength. The main drawbacks are a short signal range due to tropospheric attenuation, small target Doppler unambiguity resulting in small unambiguous target velocity measurements, and extremely short baselines in interferometric applications that make mmW ATI impractical as we will see in Section II. Sections III and IV give insight on how dual-frequency SAR increases the range of unambiguous target velocity measurements and discuss the developed monopulse processing algorithm, respectively. Section V presents experimental results with the airborne mmW SAR MEMPHIS [8]. We draw our conclusions in Section VI.

II. MONOPULSE SAR

A monopulse radar has a sum signal Σ and multiple difference signals Δ . They are the result of two, four or more separate channels sending the same radio signal at the same time (hence the term monopulse), but receiving ground return echoes independently. While Σ is the sum signal of echoes from all channels, Δ is formed from the differences thereof. These differences in amplitude as well as phase come from different viewing angles or, in the case of moving targets in SAR, from different Doppler frequencies. Fig. 1 shows a schematic view of a monopulse system with four channels A, B, C, D . In a) the difference signal will be equal to zero, meaning a target at boresight with 0 Hz Doppler frequency, while b) and c) show targets that are displaced in either azimuth or azimuth and elevation (meaning Doppler frequencies different from zero for SAR).

If we assume a channel arrangement as in Fig. 1, we may express the sum and difference signals in azimuth and elevation as

$$\Sigma = A + B + C + D, \quad (1)$$

$$\Delta_{az} = (A + C) - (B + D), \quad (2)$$

$$\Delta_{el} = (A + B) - (C + D). \quad (3)$$

Unlike a tracking radar, a SAR will only encounter targets displaced in azimuth and not in elevation [1]. The elevation difference signal Δ_{el} does not play any important role and we will ignore it in the following. Hence, when referring to Δ we will always mean the azimuth difference Δ_{az} . If we form the

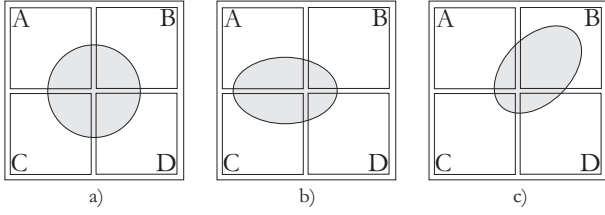


Fig. 1. Monopulse concept with a target seen by four independent receive channels A to D. In a) the target is at boresight, in b) and c) it is displaced.

signal monopulse ratio defined as

$$\text{MPR} = \frac{\Delta}{\Sigma}, \quad (4)$$

we will get zero for all boresight echoes of zero Doppler frequency, a distinct monopulse curve M from all other echoes as a function of Doppler frequency, and moving targets deviating from this curve.

A. Phase- and Amplitude Comparison

There are two different kinds of monopulse radars.

- *amplitude-comparison monopulse* consists of multiple (horn) antennas in a parabolic reflector and a single lens bundling the individual signals and giving them a common phase center. The resulting look directions of the receive channels are squinted towards each other by an angle φ_0 .
- *phase-comparison monopulse* uses multiple separate antennas looking all in the same direction with a separation baseline B resulting in independent phase centers.

The two concepts are illustrated in Fig. 2. The idea of phase-comparison monopulse is commonly used in SAR interferometry applications. However, mmW SAR systems must rely on amplitude-comparison monopulse because the physical baseline B of phase-comparison monopulse with mmW SAR gets very small and hard to be practically realizable for GMTI applications for short carrier wavelengths. For example, measurements of radial target velocities v_r from 5 to 20 m/s at a carrier wavelength λ_c of 8 mm would result in a baseline

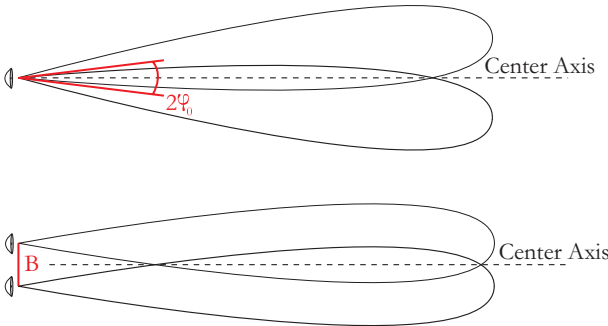


Fig. 2. Top: amplitude-comparison monopulse with one phase center and multiple squinted beams. Bottom: phase-comparison monopulse with two phase centers, parallel beams and a baseline.

of only 8 to 2 cm after the formula

$$B = \frac{\lambda_c v_s}{2 v_r} \quad (5)$$

and assuming an airborne SAR platform velocity in azimuth v_s of 100 m/s. (5) results under the condition that an optimal phase difference between physical channels would be $\lambda_c/2$. The time difference between the antenna phase centers at the same position is $t = B/v_s$ and during that time, a target will move a distance v_r/t equal to $\lambda_c/2$.

B. The MEMPHIS SAR System

MEMPHIS is an experimental airborne mmW SAR developed by FGAN-FHR [8]. Its configuration permits an amplitude-comparison monopulse mode using a lens as described above to bundle the signals from four independent horns arranged in a square. At the lens, the signals share a common phase center, but since the individual horns are separated locally from each other by a short distance, we will also get slight phase differences for moving targets in addition to intensity differences when looking at the monopulse ratios Δ/Σ .

The system operates simultaneously at both 35 and 94 GHz carrier frequency with two independent monopulse antennas and a standard signal bandwidth of 200 MHz and a pulse repetition frequency (PRF) of 1700 Hz for each antenna. Since the Doppler frequency of a target moving with radial velocity v_r is given as

$$f_d = \frac{2v_r}{\lambda_c}, \quad (6)$$

we may receive unambiguous radial velocity measurements of 7.28 m/s for $f_d < \text{PRF}$ and 35 GHz if the target movement direction is known and ± 3.64 m/s otherwise. At 94 GHz, the unambiguous velocity at 1700 Hz is 2.71 m/s or ± 1.35 m/s. All higher radial target velocities are ambiguous.

III. DUAL FREQUENCY INFORMATION

A. Theory

Ambiguous velocity measurements and, closely related, blind target speeds, are two important issues that almost always arise when looking at GMTI for mmW SAR because of high carrier frequencies. Just as velocity ambiguities are generally due to target Doppler frequency shifts outside of the PRF, blind speeds are a special case where radial target speeds are ambiguous to a 0 Hz Doppler shift because of the same aliasing effects of the limited PRF.

Reports about exploiting dual-frequency radar to resolve Doppler ambiguities date back more than 40 years. The basic idea is to resolve Doppler shifts that are multiples of the PRF for one carrier frequency by using a second frequency where the Doppler shifts are a different multiple of the PRF [9], [10]. Hence, the problem reduces to a matter of least common multiples. Today, applications for dual-frequency radar range from traditional detection of moving targets in the presence of ground clutter to wind and storm measurements in meteorology and topographic height extraction in InSAR.

Derivations of the principle include everything from dual-PRF systems [11] to dual-baseline InSAR [12].

If we apply the dual frequency technique to SAR GMTI, we are able to increase the unambiguous velocity range via the theory of least common multiples. Let us set $f_d < \text{PRF}$ in (6) and we get a new dual-frequency condition for Doppler ambiguities given as

$$\text{PRF} < \frac{2v_r}{(\lambda_{c1}, \lambda_{c2})} \quad (7)$$

where we make use of both carrier wavelengths λ_{c1} and λ_{c2} . We define $(\lambda_{c1}, \lambda_{c2})$ as the least common multiple between two values. Unfortunately, least common multiples are only defined for integer values. This will not be the case for wavelengths λ_{c1} and λ_{c2} in most dual-frequency SAR systems. The solution is to define the precision of such a system. Let us say that we trust a SAR to be precise up to x decimal digits of its wavelength in meters and we may define

$$\text{PRF} < \frac{2 \cdot v_r \cdot 10^x}{(\lambda_{c1} \cdot 10^x), (\lambda_{c2} \cdot 10^x)} \quad (8)$$

where $(\lambda_{c1} \cdot 10^x, \lambda_{c2} \cdot 10^x)$ means the nearest integer. Hence, we just expand the fractions and round off the accuracy of velocity measurements for our system.

As an example, let us use system parameters from MEMPHIS. At 35 GHz, we have a wavelength of $\lambda_{c1} = 8.57 \cdot 10^{-3}$ m and at 94 GHz one of $\lambda_{c2} = 3.19 \cdot 10^{-3}$ m. If we want three digits in the wavelength to be significant, we have to set x equal to 5. For a system PRF of 1700 Hz, we get a maximum unambiguous radial target velocity v_r of 2323.7 m/s since $(\lambda_{c1} \cdot 10^5, \lambda_{c2} \cdot 10^5) = (857, 319) = 273, 383$ m. If we restrain ourselves to a lower system precision of two significant digits for the wavelength ($x = 4$), we get $v_r = 116.9$ m/s ($(86, 32) = 1376$ m) which is still incredibly larger than the unambiguous velocities for a single frequency we got in Section II-B.

From a practical point of view, we may define a system of linear equations for a dual-frequency SAR with wavelengths λ_{c1} and λ_{c2} and measured *ambiguous* target Doppler shifts f_{d1} and f_{d2} .

$$\begin{aligned} f_{d1} &= \frac{2v_r}{\lambda_{c1}} - m \cdot \text{PRF} \\ f_{d2} &= \frac{2v_r}{\lambda_{c2}} - n \cdot \text{PRF} \end{aligned} \quad (9)$$

Of course, this system is underdetermined with unknown variable v_r and ambiguities m and n . If we assume (8) to be true, the system is solvable, but depending on the system accuracy indicated by x . Potential discrepancies between ambiguity-resolved radial target velocities v_{r1} measured at λ_{c1} and v_{r2} at λ_{c2} result in a precision indicator $\Delta\epsilon$ given as

$$\Delta\epsilon = |v_{r1} - v_{r2}|. \quad (10)$$

B. Differences in SAR Imagery

In June 2004, a GMTI experiment with the MEMPHIS SAR system was realized on the runway of the airfield in Emmen, Switzerland. Therein, five given targets were marked by Puch all-purpose vehicles with T_1 to T_3 at a nominally constant speed of 15 m/s and T_4 and T_5 at 10 m/s along the runway. Thus, they formed two independent small convoys. The front vehicle of either convoy (T_1, T_4) was equipped with a corner reflector to increase signal reception of the SAR. Two corner reflectors R_1 and R_2 were placed on the runway as well, serving as static reference targets.

The runway was imaged by MEMPHIS at 35 and 94 GHz, with 200 MHz signal bandwidth, a PRF of 1700 Hz, and a depression angle of 32° . Fig. 3 shows the 750 m wide and focused Σ signal image at 35 GHz with all targets and the corner reflectors. The targets were moving from left to right, away from the SAR sensor and are vertically displaced in the image (in azimuth). Note that the targets moving slower (T_4, T_5) are actually displaced further away from their true position in the SAR image than the ones moving faster ($T_1 - T_3$). This is exactly what happens due to the limited PRF and Doppler ambiguities implied by (6).

In Fig. 4, the focused Σ signal image at 94 GHz is shown as a comparison to Fig. 3. Note how the moving targets experience a different azimuth displacement than at 35 GHz.

IV. GMTI PROCESSING

Even if there is just one frequency available, GMTI is still possible in monopulse SAR. We developed the following algorithm to indicate moving targets and correct their position shifts in SAR. For the resolving of the true radial target velocity we are relying on (8) and the dual-frequency information.

A. Theory

While we have distinguished between amplitude- and phase-comparison monopulse methods in Section II, the data processing approach may be the same for both. Despite the misleading name, we do neither look at amplitudes or phases in monopulse processing, but always at the complex ratios Δ/Σ . To be more exact, we define the sum signal as

$$\Sigma = |\Sigma| \cdot e^{j\phi_\Sigma} \quad (11)$$

and the difference signal as

$$\Delta = |\Delta| \cdot e^{j\phi_\Delta} \quad (12)$$

to receive the complex monopulse ratios

$$\text{MPR} = \frac{\Delta}{\Sigma} = \frac{|\Delta|}{|\Sigma|} \cdot e^{j(\phi_\Delta - \phi_\Sigma)}. \quad (13)$$

Specific to SAR, there are deviations from the general monopulse processing techniques described in chapter 7 of [7]. Most important of all, we look at the processed single look complex signals $S_c(r, \omega)$ in the range-Doppler domain instead of a direct analysis of signal amplitudes. The transformations from the received echo signal $s(t, z)$ at the antenna to the

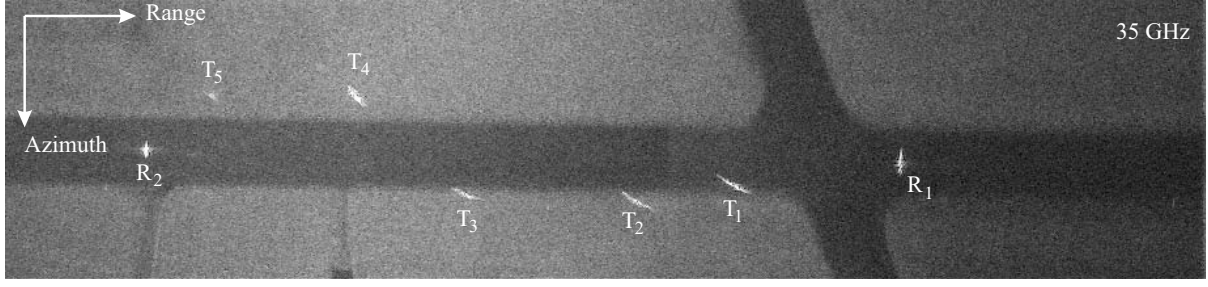


Fig. 3. 35 GHz focused SAR image of an airfield runway. The image dimensions are $750 \times 150 \text{ m}^2$ with a resolution of 0.75 m. The misplaced moving targets are moving to the right. They are marked as T_1 to T_5 and the static corner reflectors as R_1 and R_2 .



Fig. 4. 94 GHz focused SAR image recorded simultaneously to the one in (Fig. 3). Note how the moving targets are misplaced differently here than at 35 GHz because of different Doppler shifts.

processed SAR image $s_c(r, z)$ and its equivalent in the range-Doppler domain, $S_c(r, \omega)$, is

$$s(t, z) \xrightarrow{\textcircled{1}} s_c(r, z) \xrightarrow{\textcircled{2}} S_c(r, \omega) \quad (14)$$

with t the fast time, r and z distances in range und azimuth and ω the Doppler frequency. $\textcircled{1}$ stands for the SAR processing of raw data to a single look complex image (such as described in [13]). $\textcircled{2}$ is the transformation into the range-Doppler domain given by the Fourier transform.

In the following, we calculate the monopulse ratio Δ/Σ for a SAR signal in the range-Doppler domain. Therefore, we do not assume a standard $\sin(x)/x$ radar backscattering intensity of the physical channels (e. g. chapter 9 of [14]), but look at the Doppler frequency distribution at each range bin r as a standardized Gaussian distribution curve with a half-power frequency ω_p and a normalization constant $\nu = 1/\omega_p$. For simplicity reasons, we constrain ourselves to the amplitude of the complex spectra. We assume that the influence of the range r on the monopulse ratio is negligible for small image strips at large slant range distances. Thus, we define the image azimuth spectrum of the physical antenna channels independently from r as

$$S_{c_1}(\omega) = e^{-\nu^2(\omega+\omega_0)^2} \quad (15)$$

and

$$S_{c_2}(\omega) = e^{-\nu^2(\omega-\omega_0)^2}. \quad (16)$$

ω_0 is the Doppler frequency shift of the channels resulting from the squinted antenna beams as in Fig. 2. We get the Σ

und Δ signals

$$\begin{aligned} \Sigma(\omega) &= S_{c_1} + S_{c_2} \\ &= e^{-\nu^2(\omega+\omega_0)^2} + e^{-\nu^2(\omega-\omega_0)^2} \\ &= e^{-\nu^2\omega^2 - \nu^2\omega_0^2} \left(e^{2\nu^2\omega\omega_0} + e^{-2\nu^2\omega\omega_0} \right) \end{aligned} \quad (17)$$

and

$$\begin{aligned} \Delta(\omega) &= S_{c_1} - S_{c_2} \\ &= e^{-\nu^2(\omega+\omega_0)^2} - e^{-\nu^2(\omega-\omega_0)^2} \\ &= e^{-\nu^2\omega^2 - \nu^2\omega_0^2} \left(e^{2\nu^2\omega\omega_0} - e^{-2\nu^2\omega\omega_0} \right). \end{aligned} \quad (18)$$

Considering the properties of the hyperbolic functions $\sinh(x) = \frac{1}{2}(e^x - e^{-x})$ and $\cosh(x) = \frac{1}{2}(e^x + e^{-x})$ we get

$$\Sigma(\omega) = e^{-\nu^2(\omega^2+\omega_0^2)} \cdot 2 \cosh(2\nu^2\omega\omega_0) \quad (19)$$

and

$$\Delta(\omega) = e^{-\nu^2(\omega^2+\omega_0^2)} \cdot 2 \sinh(2\nu^2\omega\omega_0). \quad (20)$$

The monopulse curve of all Doppler frequencies from the static ground scene in a SAR may thus be described mathematically by a hyperbolic tangent as

$$M(\omega) = \frac{\Delta(\omega)}{\Sigma(\omega)} = \tanh(2\nu^2\omega\omega_0). \quad (21)$$

In Fig. 5, the physical channels given by (15) and (16) are plotted on the left, analogously to the situation at the top of Fig. 2, while the sum and difference signals of (17) and (18) are shown in the center and the resulting monopulse curve of (21) on the right. For this example, a total spectrum from -850 to 850 Hz was chosen corresponding to the PRF of

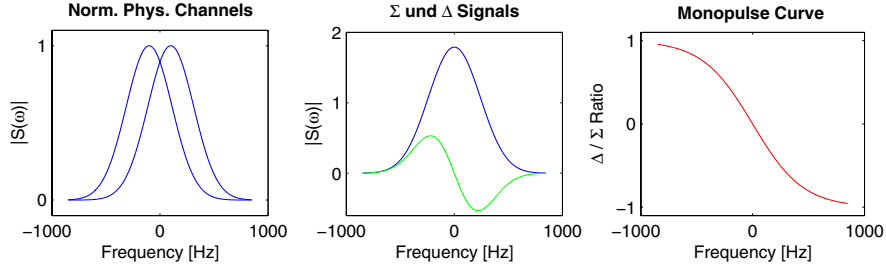


Fig. 5. The theoretical Doppler spectra of monopulse SAR — left: the normalized physical channels S_{c_1} and S_{c_2} , middle: the recorded monopulse signals of Σ and Δ , right: the monopulse curve M .

MEMPHIS with ω_p equal to 300 s^{-1} and ω_0 to 100 s^{-1} . Obviously, the slope of the monopulse curve depends on ω_0 and is thus directly related to the angle φ_0 between the physical channels. The larger φ_0 gets, the steeper the slope of Δ/Σ . This may be of an advantage when measuring very accurate target velocities with a small Doppler shift compared to the total signal spectrum. For a mmW SAR, however, the target Doppler shift will become large very fast because of the high carrier frequency, and a slight slope enables the exact measurement of a larger range of target velocities.

A moving target deviates from the monopulse curve of the static scene with the magnitude of deviation depending on the target's radial velocity component. This makes a moving target clearly discernible in the monopulse curve, regardless of whether the target's Doppler frequencies are inside or outside the clutter spectrum. Additionally, the monopulse curve of the static scene makes it possible to determine the Doppler shift of a target compared to the curve and therefore allows a correction of the azimuth displacement and estimation of the radial velocity.

B. Implementational Aspects

To be able to estimate an accurate monopulse curve $M(\omega)$ as theoretically defined in (21) from given sensor Σ and Δ signals and to identify moving targets therein, we perform the following steps including stochastic modeling of $M(\omega)$. All these steps are executed on blocks of data in the azimuth direction to avoid Doppler information from a too large sub-scene and multiple moving targets per range bin:

- 1) Because signal and SAR speckle noise may influence monopulse processing, we define an amplitude threshold and consider only Doppler frequency amplitudes in the sum signal $\Sigma(r, \omega)$ that are larger than the threshold.
- 2) We calculate and store the monopulse ratios $\text{MPR}(r, \omega) = \Delta(r, \omega)/\Sigma(r, \omega)$ over the complete Doppler spectrum for all range bins. We use only the real part of signals. The imaginary part may be considered for a phase correction later (see also chapter 3 of [7]).
- 3) Presuming independence of the monopulse ratio from range r , we calculate the mean values of $\text{MPR}(\omega)$ at all frequencies.

- 4) As shown in (21), the monopulse curve $M(\omega)$ has the form of a hyperbolic tangent. To fit a curve $M(\omega)$ through all values $\text{MPR}(\omega)$, we assume a parameterization

$$M(\omega) = a \cdot \tanh(b\omega - c) \quad (22)$$

where a , b , and c are free parameters.

- 5) We estimate a , b , and c through non-linear data modeling. A good technique is the Levenberg-Marquardt method in combination with singular value decomposition for the solution of the sets of linear equations (compare chapter 15 of [15]). Important for the method to work are well-guessed initial values of a , b , and c .
- 6) By estimating the imaginary monopulse ratios and their monopulse curve $M_{im}(\omega)$, we adjust the phase of all monopulse ratios through a multiplication of the complex Σ and Δ signals with $e^{-j\phi}$ where

$$\phi = \text{atan} \left(\frac{b_{im}}{b_{re}} \right) \quad (23)$$

and b_{re} , b_{im} are the b parameters of the real and imaginary monopulse curve.

- 7) We estimate the monopulse curve again, now with the phase-corrected ratios.
- 8) Defining a monopulse threshold, we ignore all ratios $\text{MPR}(r, \omega)$ that deviate less than the threshold from $M(\omega)$.
- 9) We determine the necessary frequency shift of all remaining signals presumed to be coming from moving targets. The frequency shifts may be directly translated into radial velocities v_r by (6), and an azimuth position correction in the image becomes possible.

Note that more than one target in the same range bin may be present if the block size of SAR images is set to be too large, complicating the algorithm. However, if it is too small, estimation of the monopulse curve $M(\omega)$ may be inaccurate.

V. EXPERIMENTAL RESULTS

The five target vehicles T_1 to T_5 of our experiment described in Section III-B were moving down the runway with their exact positions and velocities logged by GPS receivers at one second intervals. Post-measurement differential GPS processing was used to increase position and velocity data to sub-meter

accuracy. T_1 , T_2 , and T_3 were moving at 15 m/s on the lower side of the runway in Figs. 3 and 4 while T_4 and T_5 drove with 10 m/s along the upper border to avoid dangerous maneuvers between the two convoys.

Monopulse GMTI processing as described in Section IV-B gives us the spectral results shown in Fig. 6 for 35 GHz and in Fig. 7 for 94 GHz. Given are the spectra for the static reflector R_1 and targets T_1 moving at 15 m/s and T_4 at 10 m/s. The calculated monopulse ratios at the range bin of the reflector at the top left of the figure correspond very well to the estimated monopulse curve. At the bottom left, we see that no frequency remains in the spectrum after including a monopulse threshold. However, the target T_1 (middle) as well as the target T_4 (right) are clearly identified via monopulse processing. Their relative

frequency shifts are easily discernible.

Figs. 8 and 9 show the outcome in the time domain of our described monopulse algorithm for 35 and 94 GHz, respectively. All signal parts found to be static by monopulse processing have been filtered out. For orientation purposes, the airfield runway is outlined. Obviously, the target repositioning is as sensitive as the velocity estimation. An error in the velocity estimation of $\Delta v_r = 0.1$ m/s results in a position uncertainty of one meter by the relation for the displacement

$$d = \frac{v_r R}{v_a} \quad (24)$$

and assuming an aircraft velocity of $v_a = 100$ m/s and a range to the target of $R = 1000$ m.

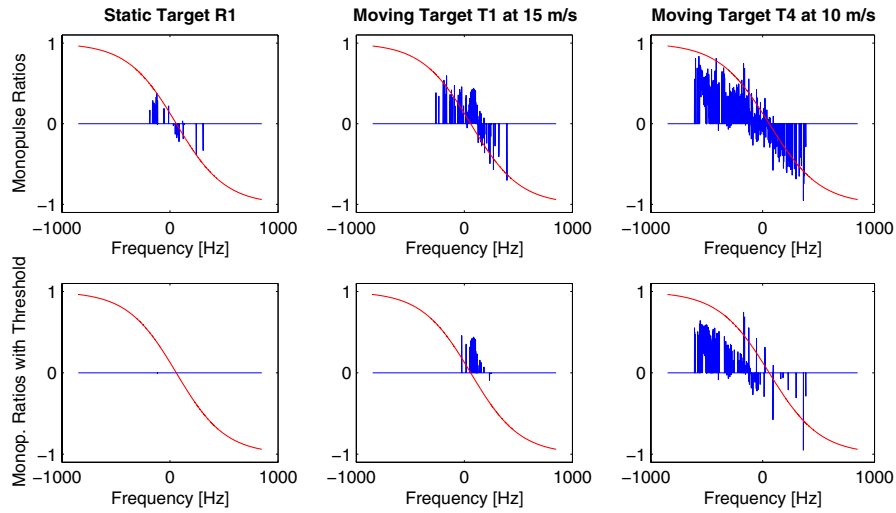


Fig. 6. Monopulse ratios at 35 GHz before (top) and after (bottom) threshold filtering. Left: Ratios of a static reflector fit on the adaptively calculated monopulse curve. Middle: Threshold filtering of the target and clutter signal (top) leaves the indication of a target moving at 15 m/s (bottom). Estimating the Doppler shift is visibly possible. Right: Indication of a second target moving at 10 m/s and showing a different Doppler shift.

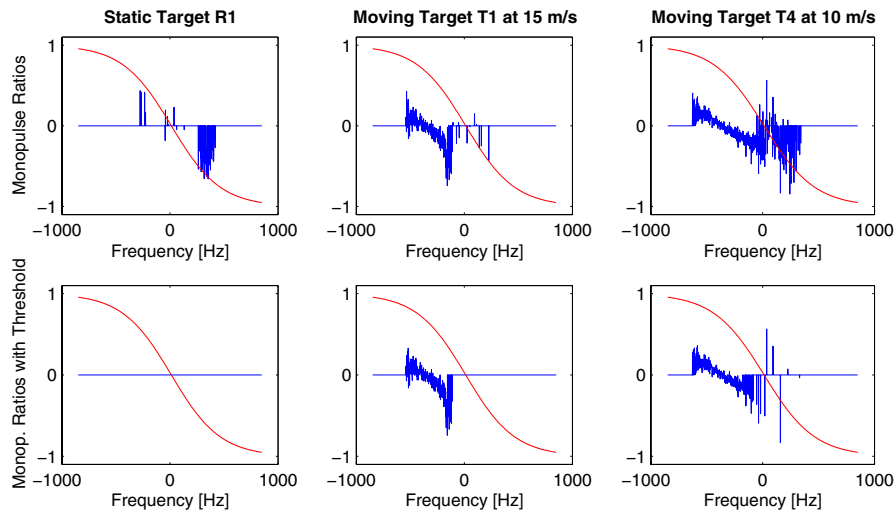


Fig. 7. Monopulse ratios at 94 GHz before (top) and after (bottom) threshold filtering for the same example targets as in Fig. 6. Left: Ratios of a static reflector fit on the adaptively calculated monopulse curve. Middle: Indication of a target moving at 15 m/s. Right: Indication of a target moving at 10 m/s.

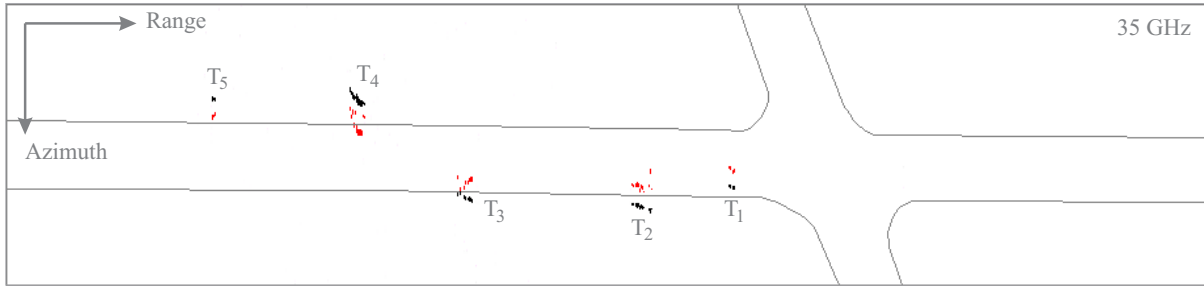


Fig. 8. Automatically indicated (black) and position-corrected (red) moving targets at 35 GHz carrier frequency. The static corner reflectors R_1 and R_2 have correctly disappeared.

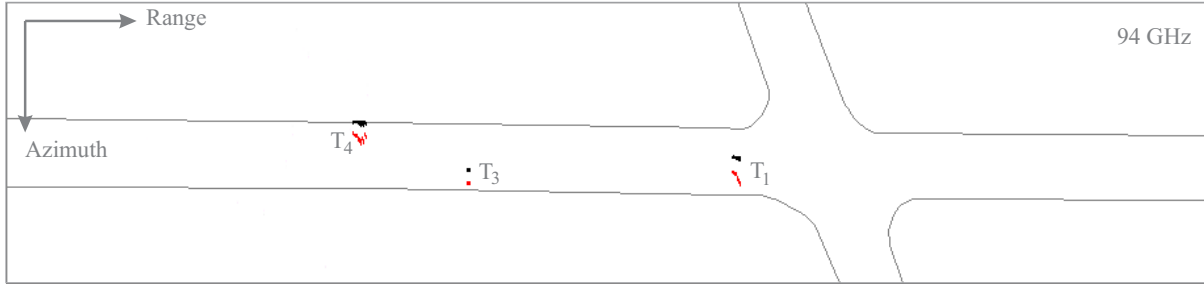


Fig. 9. Automatically indicated (black) and position-corrected (red) moving targets at 94 GHz carrier frequency. T_2 is moving with a blind speed while T_5 is too weak to be indicated.

The indicated targets appear in black and their calculated true ground positions in red. The resulting velocity components in range are listed in Tab. I and compared with calculated relative velocities between the sensor and the targets from differential GPS data. All targets are detected at 35 GHz while at 94 GHz, T_2 experienced a blind speed at the time of illumination and the target intensity of T_5 disappears in the clutter. Even at 35 GHz, T_5 is very weak and barely indicated as a moving target. The resulting velocity estimation for T_5 is worse than for the other targets. For T_1 to T_4 , velocity estimates from the monopulse processing agree very well with GPS measurements with no more than 3% deviation and displacement corrections show correct target positions.

Also, in Tab. I, we see how the velocity measurement

ambiguities indicated by the factors m and n defined in (9) could be resolved by using the dual-frequency information. We solved the system of equations (compare columns 3 and 4 in Tab. I) and assumed that the condition of the velocities being inside of the least common multiple velocity in (8) is fulfilled with $x = 4$. Obviously, we could not solve such a system for targets T_2 (blind speed at 94 GHz) and T_5 (weak signal). With our a-priori knowledge from the differential GPS measurements and by assuming two convoys of similar velocities, we filled in the corresponding ambiguity factor m and got a good velocity estimate.

For targets T_1 , T_3 , and T_4 we could determine a mean dual-frequency velocity. The deviation $\Delta\epsilon$ between the resulting ambiguity-resolved velocity at 35 and that at 94 GHz is

TABLE I

ABSOLUTE NOMINAL VALUES AND MEASURED RADIAL VELOCITIES OF MOVING TARGETS BY DIFFERENTIAL GPS AND BY THE MEMPHIS DUAL-FREQUENCY MONOPULSE SAR SENSOR. NEGATIVE VALUES INDICATE A MOVEMENT AWAY FROM THE SAR. THE NUMBERS OF DOPPLER AMBIGUITIES m AND n ARE RESOLVED VIA LEAST COMMON MULTIPLES TO GET THE DUAL-FREQUENCY VELOCITY ESTIMATE. $\Delta\epsilon$ IS THE DEVIATION BETWEEN THE 35 AND 94 GHz VELOCITY MEASUREMENT GIVEN IN (10).

| Target | Nom. Velocity (ground) [m/s] | 35 GHz SAR Vel (radial) [m/s] | 94 GHz SAR Vel (radial) [m/s] | m | n | $\Delta\epsilon$ [m/s] | Mean Dual-Freq Vel (radial) [m/s] | GPS Vel (radial) [m/s] | Δ SAR-GPS [m/s] |
|--------|------------------------------|-------------------------------|-------------------------------|-----|-----|------------------------|-----------------------------------|------------------------|------------------------|
| T_1 | 15 | $0.57 + m \cdot 7.28$ | $-0.64 + n \cdot 2.71$ | -2 | -5 | 0.2 | -14.1 | -14.4 | 0.3 |
| T_2 | 15 | $0.66 + m \cdot 7.28$ | blind | -2 | — | — | -13.9 | -14.0 | 0.1 |
| T_3 | 15 | $0.73 + m \cdot 7.28$ | $-0.46 + n \cdot 2.71$ | -2 | -5 | 0.2 | -13.9 | -14.2 | 0.3 |
| T_4 | 10 | $-1.05 + m \cdot 7.28$ | $-0.58 + n \cdot 2.71$ | -1 | -3 | 0.4 | -8.5 | -8.8 | 0.3 |
| T_5 | 10 | $-0.64 + m \cdot 7.28$ | too weak | -1 | — | — | -7.9 | -8.7 | 0.8 |

of the same order as that one between the SAR and GPS measurements, indicating that our MTI algorithms worked fine at both frequencies.

VI. CONCLUSION

For mmW SAR systems, amplitude-comparison monopulse data recording is a very effective GMTI technique that solves the dilemma of extremely short interferometric mmW baselines. It is a sound method with multiple channels sharing a single phase center. The basic concept is well-known from tracking radar applications and directly transferable to SAR GMTI scenarios.

Processing of monopulse data for SAR GMTI includes a mathematically complex nonlinear data modeling step to fit received and compressed signals to a stochastically determined hyperbolic tangent function in the range Doppler domain. Resulting deviations of moving targets from this function and thus from the static scene are well detectable and compensable, allowing for exact radial target velocity calculations and position shift corrections.

When calculating radial target velocities, a general problem for mmW SAR MTI are high Doppler frequency shifts from the detected targets even at velocities of a few meters or less per second. PRF requirements for unambiguous velocity measurements would be exceedingly high. Using dual-frequency information, the concern about high PRF requirements is eliminated via the theory of least common multiples for the single velocity ambiguities. Indication of targets is very sensitive, and accurate position correction are possible.

Our experimental results obtained with the presented processing algorithm show the effectiveness of monopulse processing for SAR. Monopulse processing of the Δ/Σ Doppler signal ratios makes use of real as well as imaginary signal information. Velocity estimates and target displacement correction are accurate and fully automatically possible via monopulse ratio comparison of targets with our presented method of estimating a monopulse curve for the static scene. We could show that the theoretical hyperbolic tangent monopulse curve fits very well to measured static corner reflector data, giving proof to the practical application of our modeling approach and also to theory of dual-frequency SAR.

ACKNOWLEDGMENT

We would like to thank the procurement and technology center of the Swiss Federal Department of Defence (*armasuisse*) and especially Peter Wellig for their wide support and cooperation.

REFERENCES

- [1] R. K. Raney, "Synthetic Aperture Imaging Radar and Moving Targets," *IEEE Trans. Aerosp. Electron. Syst.*, vol. 7, pp. 499–505, May 1971.
- [2] S. R. J. Axelsson, "Position Correction of Moving Targets in SAR-Imagery," in *Proc. SPIE*, vol. 5236, Barcelona, Jan. 2004, pp. 80–92.
- [3] S. Chiu and C. E. Livingstone, "A Comparison of Displaced Phase Centre Antenna and Along-Track Interferometry Techniques for RADARSAT-2 Ground Moving Target Indication," *Canad. J. Remote Sensing*, vol. 31, no. 1, pp. 37–51, Feb. 2005.
- [4] J. H. G. Ender, "Space-time Processing for Multichannel Synthetic Aperture Radar," *Electronics and Communication Eng. J.*, pp. 29–38, Feb. 1999.
- [5] M. Soumekh, "Moving Target Detection and Imaging Using an X-Band Along-Track Monopulse SAR," *IEEE Trans. Aerosp. Electron. Syst.*, vol. 38, no. 1, pp. 315–333, Jan. 2002.
- [6] R. Romeiser, H. Breit, M. Eineder, H. Runge, P. Flament, K. de Jong, and J. Vogelzang, "Current Measurements by SAR Along-Track Interferometry from a Space Shuttle," *IEEE Trans. Geosci. Remote Sensing*, vol. 43, no. 10, pp. 2315–2324, Oct. 2005.
- [7] S. M. Sherman, *Monopulse Principles and Techniques*. Boston: Artech House Publishers, 1984.
- [8] H. Schimpf, H. Essen, S. Böhmendorf, and T. Brehm, "MEMPHIS - A Fully Polarimetric Experimental Radar," in *Proc. IGARSS*, vol. 3, Toronto, June 2002, pp. 1714–1716.
- [9] R. J. Doviak, D. S. Zrnic, and D. S. Sirmans, "Doppler Weather Radar," *Proc. IEEE*, vol. 67, no. 22, pp. 1522–1553, Nov. 1979.
- [10] L. S. Miller, E. L. Sheppard, G. M. Heymsfield, and P. Racette, "A Technique for Resolving Range-Doppler Ambiguities at Microwave, Millimeter, or Optical Wavelengths," in *IEEE Proc. Southeastcon '93*, Charlotte, Apr. 1993, pp. 1–2.
- [11] D. P. Jorgensen, T. R. Shepherd, and A. S. Goldstein, "A Dual-Pulse Repetition Frequency Scheme for Mitigating Velocity Ambiguities of the NOAA P-3 Airborne Doppler Radar," *J. Atmos. and Ocean. Tech.*, vol. 17, no. 5, p. 585594, May 2000.
- [12] G. Corsini, M. Diani, F. Lombardini, and G. Pinelli, "Simulated Analysis and Optimization of a Three-Antenna Airborne InSAR System for Topographic Mapping," *IEEE Trans. Geosci. Remote Sensing*, vol. 37, no. 5, pp. 2518–2529, Sept. 1999.
- [13] R. Bamler, "A Comparison of Range-Doppler and Wavenumber Domain SAR Focusing Algorithms," *IEEE Trans. Geosci. Remote Sensing*, vol. 30, no. 4, pp. 706–713, July 1992.
- [14] B. R. Mahafza and A. Z. Elsherbeni, *Matlab Simulations for Radar System Design*. Boca Raton: Chapman & Hall / CRC, 2004.
- [15] W. H. Press, B. P. Flannery, S. A. Teukolsky, and W. T. Vetterling, *Numerical Recipes in C: The Art of Scientific Computing, Second Edition*. Cambridge: Cambridge University Press, 1992.